

Development of a temperature-controlled phantom for magnetic resonance quality assurance of diffusion, dynamic, and relaxometry measurements

Neil P. Jerome, Marianthi-Vasiliki Papoutsaki, Matthew R. Orton, Harold G. Parkes, Jessica M. Winfield, Michael A. Boss, Martin O. Leach, Nandita M. deSouza, and David J. Collins

Citation: *Medical Physics* **43**, 2998 (2016); doi: 10.1118/1.4948997

View online: <http://dx.doi.org/10.1118/1.4948997>

View Table of Contents: <http://scitation.aip.org/content/aapm/journal/medphys/43/6?ver=pdfcov>

Published by the [American Association of Physicists in Medicine](#)

Articles you may be interested in

[Design and testing of a phantom and instrumented gynecological applicator based on GaN dosimeter for use in high dose rate brachytherapy quality assurance](#)

Med. Phys. **43**, 5240 (2016); 10.1118/1.4961393

[Development and clinical evaluation of an ionization chamber array with 3.5 mm pixel pitch for quality assurance in advanced radiotherapy techniques](#)

Med. Phys. **43**, 2283 (2016); 10.1118/1.4945414

[Diffusion tensor imaging using a high-temperature superconducting resonator in a 3 T magnetic resonance imaging for a spontaneous rat brain tumor](#)

Appl. Phys. Lett. **102**, 063701 (2013); 10.1063/1.4790115

[A proposed scheme for comprehensive characterization of the measured geometric distortion in magnetic resonance imaging using a three-dimensional phantom](#)

Med. Phys. **31**, 2212 (2004); 10.1118/1.1767051

[Porous phantoms for PET and SPECT performance evaluation and quality assurance](#)

Med. Phys. **31**, 1183 (2004); 10.1118/1.1711416

**THERE ARE SO MANY POTENTIAL
HOLES IN THE PROCESS FOR
RADIOTHERAPY QA...**

See how SunCHECK™ is integrating patient safety in radiation oncology >>

 **SUN NUCLEAR**
corporation



Development of a temperature-controlled phantom for magnetic resonance quality assurance of diffusion, dynamic, and relaxometry measurements

Neil P. Jerome^{a)}

Cancer Research UK Cancer Imaging Centre, Division of Radiotherapy and Imaging, The Institute of Cancer Research and Royal Marsden Hospital, 123 Old Brompton Road, London SM2 5NG, United Kingdom

Marianthi-Vasiliki Papoutsaki^{a),b)}

Cancer Research UK Cancer Imaging Centre, Division of Radiotherapy and Imaging, The Institute of Cancer Research and Royal Marsden Hospital, 123 Old Brompton Road, London SM2 5NG, United Kingdom and Members of the Quantitative Imaging in Cancer: Connecting Cellular Processes with Therapy (QuiC-ConCePT) Consortium

Matthew R. Orton, Harold G. Parkes, and Jessica M. Winfield

Cancer Research UK Cancer Imaging Centre, Division of Radiotherapy and Imaging, The Institute of Cancer Research and Royal Marsden Hospital, 123 Old Brompton Road, London SM2 5NG, United Kingdom

Michael A. Boss

National Institute of Standards and Technology, 325 Broadway, Boulder, Colorado 80305

Martin O. Leach

Cancer Research UK Cancer Imaging Centre, Division of Radiotherapy and Imaging, The Institute of Cancer Research and Royal Marsden Hospital, 123 Old Brompton Road, London SM2 5NG, United Kingdom

Nandita M. deSouza

Cancer Research UK Cancer Imaging Centre, Division of Radiotherapy and Imaging, The Institute of Cancer Research and Royal Marsden Hospital, 123 Old Brompton Road, London SM2 5NG, United Kingdom and Members of the Quantitative Imaging in Cancer: Connecting Cellular Processes with Therapy (QuiC-ConCePT) Consortium

David J. Collins

Cancer Research UK Cancer Imaging Centre, Division of Radiotherapy and Imaging, The Institute of Cancer Research and Royal Marsden Hospital, 123 Old Brompton Road, London SM2 5NG, United Kingdom

(Received 10 August 2015; revised 20 April 2016; accepted for publication 28 April 2016; published 20 May 2016)

Purpose: Diffusion-weighted (DW) and dynamic contrast-enhanced magnetic resonance imaging (MRI) are increasingly applied for the assessment of functional tissue biomarkers for diagnosis, lesion characterization, or for monitoring of treatment response. However, these techniques are vulnerable to the influence of various factors, so there is a necessity for a standardized MR quality assurance procedure utilizing a phantom to facilitate the reliable estimation of repeatability of these quantitative biomarkers arising from technical factors (e.g., B_1 variation) affecting acquisition on scanners of different vendors and field strengths. The purpose of this study is to present a novel phantom designed for use in quality assurance for multicenter trials, and the associated repeatability measurements of functional and quantitative imaging protocols across different MR vendors and field strengths.

Methods: A cylindrical acrylic phantom was manufactured containing 7 vials of polyvinylpyrrolidone (PVP) solutions of different concentrations, ranging from 0% (distilled water) to 25% w/w, to create a range of different MR contrast parameters. Temperature control was achieved by equilibration with ice-water. Repeated MR imaging measurements of the phantom were performed on four clinical scanners (two at 1.5 T, two at 3.0 T; two vendors) using the same scanning protocol to assess the long-term and short-term repeatability. The scanning protocol consisted of DW measurements, inversion recovery (IR) T_1 measurements, multiecho T_2 measurement, and dynamic T_1 -weighted sequence allowing multiple variable flip angle (VFA) estimation of T_1 values over time. For each measurement, the corresponding calculated parameter maps were produced. On each calculated map, regions of interest (ROIs) were drawn within each vial and the median value of these voxels was assessed. For the dynamic data, the autocorrelation function and their variance were calculated; for the assessment of the repeatability, the coefficients of variation (CoV) were calculated.

Results: For both field strengths across the available vendors, the apparent diffusion coefficient (ADC) at 0 °C ranged from $(1.12 \pm 0.01) \times 10^{-3}$ mm²/s for pure water to $(0.48 \pm 0.02) \times 10^{-3}$ mm²/s for the 25% w/w PVP concentration, presenting a minor variability between the vendors and the field strengths. T_2 and IR- T_1 relaxation time results demonstrated variability between the field strengths and the vendors across the different acquisitions. Moreover, the T_1 values derived from the VFA method

exhibited a large variation compared with the IR- T_1 values across all the scanners for all repeated measurements, although the calculation of the standard deviation of the VFA- T_1 estimate across each ROI and the autocorrelation showed a stability of the signal for three scanners, with autocorrelation of the signal over the dynamic series revealing a periodic variation in one scanner. Finally, the ADC, the T_2 , and the IR- T_1 values exhibited an excellent repeatability across the scanners, whereas for the dynamic data, the CoVs were higher.

Conclusions: The combination of a novel PVP phantom, with multiple compartments to give a physiologically relevant range of ADC and T_1 values, together with ice-water as a temperature-controlled medium, allows reliable quality assurance measurements that can be used to measure agreement between MRI scanners, critical in multicenter functional and quantitative imaging studies. © 2016 Author(s). All article content, except where otherwise noted, is licensed under a Creative Commons Attribution (CC BY) license (<http://creativecommons.org/licenses/by/4.0/>). [<http://dx.doi.org/10.1118/1.4948997>]

Key words: quality assurance, diffusion weighted imaging, quantitative imaging

1. INTRODUCTION

Magnetic resonance imaging (MRI) is a powerful noninvasive imaging modality in oncology. Functional information on tissue structure gained from diffusion-weighted (DW) and dynamic contrast-enhanced (DCE) sequences is increasingly used to yield observations beyond lesion size and location. DW-MRI gives signal contrast derived from random motion of water molecules in biological tissues and depends on tissue structure; the derived apparent diffusion coefficient (ADC) is also modulated by the presence of macromolecules, interactions with cell membranes, and flow within vessels.^{1,2} The sensitivity of this technique to water diffusion properties of tissue is generated by application of gradient pulses of varying amplitudes, separations, and durations, summarized by the parameter known as the b -value. In practice b -values are selected not only by consideration of the anatomical region being evaluated but also by the system capabilities and even the investigator's preferences.

DCE-MRI uses the kinetics of an administered exogenous contrast agent to assess characteristics of tumor vasculature. Pharmacokinetic modeling of the signal intensity curve over repeated T_1 -weighted scans [utilizing a rapid T_1 -weighted gradient-echo acquisition method as used for the variable flip angle (VFA) measurements] with sufficient time resolution following modeling gives parameters such as forward transfer constant (K^{trans}) and rate constant (k_{ep}) between extracellular extravascular space and plasma, and fractional volumes of extracellular extravascular space (v_e) and blood plasma (v_p) per unit volume of tissue. Model-independent parameters can also be obtained from the DCE-MRI measurement, such as initial area under the gadolinium curve over 60 s after arrival of contrast agent (IAUGC60) and the precontrast longitudinal relaxation time (precontrast T_1). Precontrast T_1 is calculated using the VFA method with one or more (precontrast) volume from the dynamic scan and a matched volume acquired with a distinct (usually lower) flip angle.³

Although DW-MRI (Refs. 4–6) and DCE-MRI are valuable modalities in functional imaging,^{7–10} they are susceptible to the influence of various factors including scanner type, field strength, hardware specifications, and software implemen-

tation. Understanding the repeatability and the variability of these measurements is critical if these modalities are to be used in a quantitative manner for the prediction or monitoring of treatment response in clinical trials, particularly in pediatric trials where the relative rarity of disease requires participation of multiple centers. A standardized MR quality assurance procedure with a test object, or “phantom,” applied to various scanners of different vendors and field strengths with a repeatability estimate, would facilitate the reliable use of these quantitative results as biomarkers.

An ideal phantom must provide reliable and reproducible multiparameter measurements without any temperature dependence. Ideally, phantoms¹¹ should be made of materials that (a) provide values relevant to physiological ranges, (b) are easily prepared, inexpensive, stable over time, and nontoxic, and (c) provide reliable and reproducible values. There is no currently available phantom that satisfies all of these requirements. Pierpaoli *et al.*¹² first introduced solutions of polyvinylpyrrolidone (PVP) in water as potential phantoms for DW-MRI measurements, though without temperature control. PVP is an organic polymer, and by varying its concentration in solution, a range of desirable T_1 and ADC values can be created without the addition of any paramagnetic metal ions. Additionally, PVP solutions are known to be chemically stable over a long period of time, in contrast to the sucrose solutions previously used for quality assurance of diffusion measurements.^{13,14} Malyarenko *et al.*¹⁵ used ice-water as a universal temperature control fluid in diffusion measurements, removing the need to adjust for the known temperature dependence of T_1 and ADC values. Subsequently, Boss *et al.*¹⁶ proposed an ice-water temperature-controlled phantom with PVP solutions for the quality assurance of diffusion measurements providing reliable and repeatable values relevant to the physiological range. For DCE-MRI, different dynamic phantoms have been presented for specific applications;¹⁷ a general-purposed phantom providing a physiological range of T_1 values for assessment of stability with controlled temperature would be ideal for deriving comparative metrics across different MR vendors.

A standardized MR quality assurance procedure, combining a protocol for performing multiple functional MRI

measurements (like DW and DCE-MRI) in a limited time with a well-designed phantom of multiple temperature-controlled solutions with a suitable range of multiple MR contrast parameters, will provide a valuable resource for multicenter imaging protocol development and optimization within multicenter trials. The aim of this study is therefore to present such a phantom and the repeatability measurements of functional, DW and DCE-MRI, and quantitative T_1 and T_2 , imaging protocols across different MR vendors and field strengths as a quality assurance tool in multicenter clinical trials.

2. MATERIALS AND METHODS

2.A. Phantom preparation

Polyvinylpyrrolidone [PVP, $(C_6H_9NO)_x$, Sigma-Aldrich] with a mean molar mass of 55 000 g/mol was used for the generation of gels with different MR characteristics. Materials for construction of the phantom are inexpensive and readily available, and construction itself is approximately one day's labor. PVP in powder form was dissolved in 320 ml of distilled water inside a water bath in order to prepare the mixture under constant temperature conditions ($55^\circ C$). The solution was continuously stirred until the PVP was fully dissolved and then left in the water bath for 45 min to stabilize, before being removed and left to cool to room temperature ($18^\circ C$). Different amounts of this stock solution were diluted in distilled water for the production of PVP concentration solutions ranging from 2.5% to 25% w/w. Each solution was degassed using He in order to remove any dissolved oxygen. All the solutions were produced under the same conditions, to reduce systematic error on the MR measurements. In the initial preparation, containing only PVP and distilled water, bacterial growth was observed four months following production; the whole procedure was thus repeated with the inclusion of sodium azide (5 mg) to the initial PVP mixture to prevent this growth. The different concentrations were transferred to 60 ml vials (diameter 27 mm), and these were sealed using their appropriate caps and paraffin film.

Six different PVP solutions with concentrations 2.5%, 5%, 10%, 15%, 20%, and 25% w/w, together with one vial containing distilled water (0%, with sodium azide) and a localization rod were fixed inside a custom-built cylindrical acrylic phantom, with an inner diameter of 18 cm and height of 19 cm. The vial with the distilled water was positioned in the center of the phantom and the PVP vials arranged such that when viewed axially, PVP concentration decreased counterclockwise (Fig. 1).

Temperature control of the phantom was achieved by filling the cylinder with ice-water 1 h before scanning. Following a 45-min equilibration time, more ice was added to replenish the amount melted. Before transferring the phantom to the MR scanner room, the temperature was measured to verify that the phantom contents were at $0^\circ C$.

2.B. MRI acquisition

MR imaging measurements were performed on four clinical scanners, two at 1.5 T, denoted scanners A (MAGNETOM Avanto, Siemens Healthcare, Erlangen, Germany) and B (MAGNETOM Aera, Siemens Healthcare, Erlangen, Germany) and two at 3.0 T, denoted C (MAGNETOM Skyra, Siemens Healthcare, Erlangen, Germany) and D (Achieva, Philips Healthcare, Best, The Netherlands), using the appropriate modified protocol for each case. The scanning protocol included DW-MRI, inversion recovery T_1 measurements (IR- T_1), a multiecho T_2 measurement, and a dynamic scan as used for DCE-MRI allowing variable flip angle estimation of T_1 (VFA- T_1) with successive dynamic volumes. The scanning parameters for these scans on each system are presented in Tables I–IV. For DW-MRI, four separate successive measurements were acquired and stored separately to avoid signal averaging in the scanner and allow investigation of measurement stability. The flip angles for the VFA measurement were determined as optimal for the expected range of T_1 (500–1400 ms) in the phantom at 1.5 T.^{18,19}

The phantom was placed on the scanner bed with its central axis parallel to the z -axis of the magnet for axial image

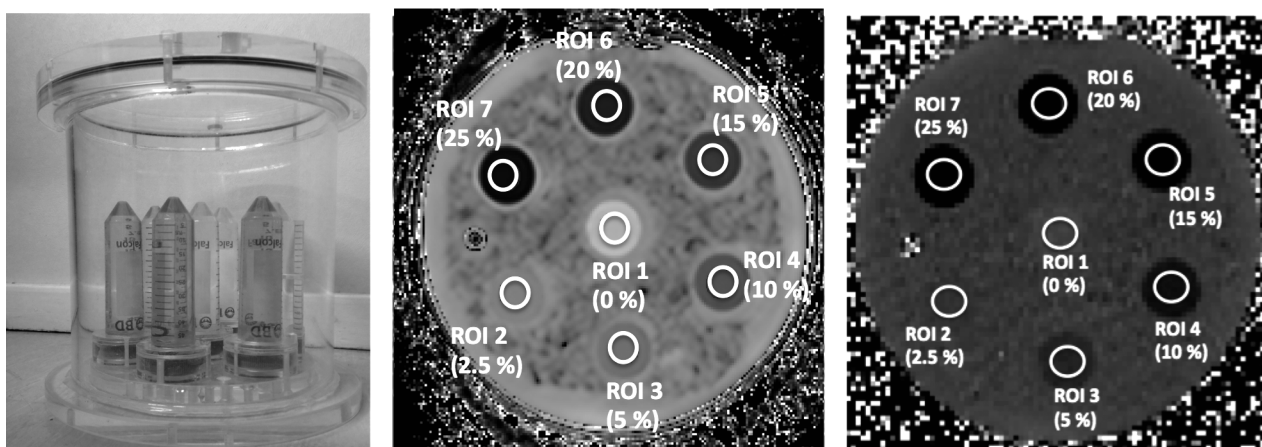


FIG. 1. Phantom construction with PVP gels (left), calculated axial T_2 map (center, T_2 range from 510 to 1406 ms), and calculated axial T_1 map (right, T_1 range from 520 to 1415 ms) of the phantom at 1.5 T with the selected ROIs with corresponding PVP concentrations are given in % w/w.

TABLE I. Sequence parameters for acquisition of diffusion-weighted imaging measurements.

	A (1.5 T)	B (1.5 T)	C (3.0 T)	D (3.0 T)
Type of sequence	Single-shot echo planar imaging			
Coil	Body array coil	Body array coil	Body array coil	Torso coil
Number of slices	5	5	5	5
Slice thickness (mm)	5	5	5	5
Gap slice (mm)	0	0	0	0
Orientation	Axial	Axial	Axial	Axial
FoV (mm)	320 × 280	320 × 280	320 × 260	320 × 320
Acquired matrix	128 × 112	128 × 112	128 × 104	128 × 128
Reconstructed matrix	256 × 224	256 × 224	256 × 208	128 × 128
Parallel imaging	GRAPPA	GRAPPA	GRAPPA	SENSE
PE direction	Right–left	Right–left	Right–left	Right–left
TR (ms)	8000	8000	8000	8000
TE (ms)	76	76	76	76
b (mm ² s)	0, 100, 500, 900	0, 100, 500, 900	0, 100, 500, 900	0, 100, 500, 900
Diffusion gradient mode	3 scan trace	3 scan trace	3 scan trace	Gradient overplus
Receiver bandwidth (Hz/pixel)	1776	1775	1775	2996
NSA	4 (separate)	4 (separate)	4 (separate)	4 (separate)
Fat-suppression technique	SPAIR	SPAIR	SPAIR	SPAIR

acquisition. To ensure the reproducible positioning of the phantom on the bed across the repeatable measurements, the internal localization rod was used as a localization reference. A plastic wedge was used to slightly raise one end of the phantom, in order to force any bubbles to the top of the phantom and remove them from the field of view (FoV). The phantom was scanned three times on each scanner in separate imaging sessions to assess both long-term and short-term repeatability of DW, DCE, T_1 , and T_2 measurements, using paired scans separated by approximately 1 month and 2–24 h (with complete removal and repositioning of the phantom and routine scanning performed in between), respectively. In each case, the scanning duration was 50 min, during which period the temperature of the phantom components was between 0 and 1 °C.

2.C. Data analysis

All calculations of functional parameters were performed on a voxel-by-voxel basis, with no image smoothing, using in-house software (ADEPT and MRIW, Institute of Cancer Research, London). For all calculated parameter maps, large circular regions of interest (ROIs) (area 138–250 mm²) were drawn within each vial in the phantom, and the median value for the voxels in each ROI recorded. ADC and T_2 maps were calculated using a monoexponential model for all b -value and echo time images, respectively [Eqs. (1) and (2)]. T_1 maps were calculated using the images acquired at different inversion times (IR- T_1) according to Eq. (3) (valid given the long TR of 10 s) and then separately using the variable flip angle method, using a combination of the multiple-averaged data at low flip

TABLE II. Sequence parameters for acquisition of inversion recovery T_1 (IR- T_1) measurements.

	A (1.5 T)	B (1.5 T)	C (3.0 T)	D (3.0 T)
Sequence	Turbo flash	Turbo flash	Turbo flash	Turbo flash
Coil	Body array	Body array	Body array	Torso
Number of slices	1	1	1	1
Slice thickness (mm)	8	8	8	8
Orientation	Axial	Axial	Axial	Axial
FoV (mm)	300 × 300	300 × 300	300 × 300	300 × 300
Acquired matrix	128 × 102	128 × 102	128 × 102	120 × 120
Reconstructed matrix	128 × 128	128 × 128	128 × 128	128 × 128
TR (ms)	10 000	10 000	10 000	10 000
TE (ms)	1.2	1.2	1.2	1.6
Receiver bandwidth (Hz/pixel)	488	490	490	479
NSA	1	1	1	1
Fat-suppression technique	Inversion recovery	Inversion recovery	Inversion recovery	Inversion recovery
Inversion times (s)	0.11, 0.3, 0.4, 0.5, 0.7, 0.9, 1.1, 1.3, 1.5, 2, 2.5, 3, 3.5, 4, 4.5	0.11, 0.3, 0.4, 0.5, 0.7, 0.9, 1.1, 1.3, 1.5, 2, 2.5, 3, 3.5, 4, 4.5	0.11, 0.3, 0.4, 0.5, 0.7, 0.9, 1.1, 1.3, 1.5, 2, 2.5, 3, 3.5, 4, 4.5	0.15, 0.3, 0.4, 0.5, 0.7, 0.9, 1.1, 1.3, 1.5, 2, 2.5, 3, 3.5, 4, 4.5

TABLE III. Sequence parameters for acquisition of variable flip angle T_1 (VFA- T_1) measurements.

	A (1.5 T)	B (1.5 T)	C (3.0 T)	D (3.0 T)
Type of sequence	3D flash	3D flash	3D flash	Spoiled 3D GRE
Coil	Body array	Body array	Body array	Torso
Number of slices	14	18	18	14
Slice thickness (mm)	5	5	5	5
Orientation	Axial	Axial	Axial	Axial
FoV (mm)	301 × 301	230 × 230	280 × 227	350 × 350
Acquired matrix	128 × 96	128 × 83	128 × 84	128 × 130
Reconstructed matrix	128 × 96	128 × 128	128 × 104	128 × 130
TR (ms)	3.00	3.32	3.32	3.70
TE (ms)	0.91	0.71	0.75	1.723
Receiver bandwidth (Hz/pixel)	651	600	600	498
NSA: static, dynamic	10, 80 × 1	4, 80 × 1	4, 80 × 1	10, 80 × 1
Flip angles (deg)	2, 11	2, 11	2, 11	2, 11

angle with each of the images in the dynamic series at higher flip angle (VFA- T_1) according to Eq. (4),

$$S_{(b)} = S_0 \exp(-b \cdot \text{ADC}), \quad (1)$$

$$S_{(\text{TE})} = S_0 \exp\left(\frac{-\text{TE}}{T_2}\right), \quad (2)$$

$$S_{(\text{TI})} = S_0 \cdot \left[1 - 2 \cdot \exp\left(\frac{-\text{TI}}{T_1}\right)\right], \quad (3)$$

$$\frac{S_n}{\sin\theta_n} = \exp\left(\frac{-\text{TR}}{T_1}\right) \cdot \frac{S_n}{\tan\theta_n} + S_0 \cdot \left[1 - \exp\left(\frac{-\text{TR}}{T_1}\right)\right]. \quad (4)$$

To confirm good signal-to-noise ratios (SNRs) for derived parameters from the diffusion-weighted and T_2 -weighted measurements, SNRs were estimated for the vial with the largest ADC at highest b -value and for the vial with the shortest T_2 at longest echo for the 4 scanners using the average signal within the ROI divided by the variance of noise from a corresponding region ROI positioned in empty space (devoid of artefacts) on the same image.

TABLE IV. Sequence parameters for acquisition of T_2 measurements.

	A (1.5 T)	B (1.5 T)	C (3.0 T)	D (3.0 T)
Type of sequence	Multiple spin echo	Multiple spin echo	Multiple spin echo	Multiple spin echo
Coil	Body array	Body array	Body array	Torso
Number of slices	1	1	1	1
Slice thickness (mm)	8	8	8	8
Orientation	Axial	Axial	Axial	Axial
FoV (mm)	300 × 262	300 × 262	300 × 262	300 × 300
Acquired matrix	128 × 112	128 × 112	128 × 112	120 × 120
Reconstructed matrix	256 × 224	256 × 224	256 × 224	224 × 224
TR (ms)	4000	4000	4000	4000
TE (ms)	13.1, 26.2, 39.3, ..., 419.2 (32 values)	13.1, 26.2, 39.3, ..., 419.2 (32 values)	13.1, 26.2, 39.3, ..., 419.2 (32 values)	13, 26, 39, ..., 416 (32 values)
Receiver bandwidth (Hz/pixel)	130	130	130	1620
NSA	1	1	1	1

From the dynamic data, it is also possible to calculate the autocorrelation (AC) function for each T_1 measurement to its successive measure, as well as the variance of the T_1 measurement across the whole dynamic series, yielding the T_1 noise factor (T_1 NF), Eq. (5),²⁰ and T_1 SNR, Eq. (6),²¹

$$T_1 \text{NF} = \left[\frac{\sigma_{T_1}}{T_1} \middle/ \frac{\sigma_S}{S_0} \right], \quad (5)$$

$$T_1 \text{SNR} = \frac{T_1}{\sigma_{T_1} \sqrt{T_S}}, \quad (6)$$

where σ_{T_1} and σ_S are the standard deviations (s.d.) of T_1 and the signal, respectively, S_0 is the initial signal intensity, and T_S is the total scan time.

2.D. Statistical analysis

The short-term and long-term repeatability of each MR contrast parameter were assessed using the repeated measurements coefficient of variation (CoV, expressed as percentage) between the second and the third imaging session (time separation between 2 and 24 h, with complete removal and repositioning of the phantom) and between the first and the second imaging session (time separation more than 1 month), respectively. For the calculation of the CoVs, a log-normal distribution was assumed and logarithms of the parameters were used when calculating the various statistics.^{22,23} First, the sample variance (V) of the logarithmic difference of the two compared imaging sessions were calculated, and then the CoV (%) was assessed by the following equation:

$$\text{CoV} = 100\% \times \sqrt{\exp\left(\frac{V}{2}\right) - 1}. \quad (7)$$

3. RESULTS

3.A. Apparent diffusion coefficient values

For each vendor, four individual diffusion-weighted measurements were acquired, the SNR of the highest b -

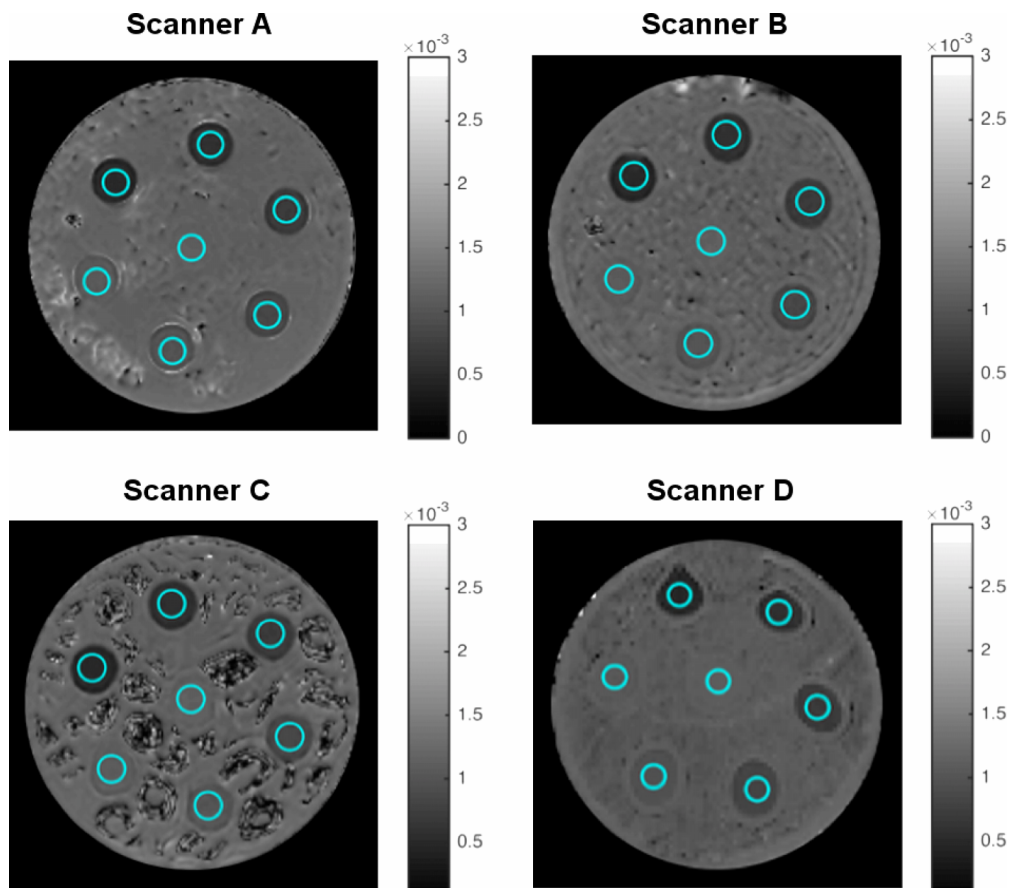


Fig. 2. Representative ADC maps for each scanner, A and B at 1.5 T and C and D at 3.0 T. The calculated values of ADC showed excellent repeatability and reproducibility across scanners.

value image on the central vial (0% w/w PVP solution) was estimated [ranged from 147.2 to 3155.8 (signal/noise)], and the mean voxel signal intensity at each voxel for all images for each b -value was calculated for the production of the ADC maps (Fig. 2). As presented in Table I, the field of view of scanner D was different to the other scanners, reflecting current clinical protocol variation. The ADC values of each vial were estimated using each of the four individual measurements (nonaveraged, acquired within a single imaging session) and using the mean of these measurements. The percentage deviations of the ADC estimates in each vial between the mean and each individual measurement were less than 1%, indicating low intrinsic measurement noise. Moreover, the percentage deviations between the ADC estimates of each slice and the corresponding estimates of all the slices were also less than 1%, showing negligible variation through the slices. Consequently, the ADC values reported are the mean values at each of the four acquisitions (nonaveraged measurements) on each scanner for one imaging session, from the central slice (Table V). At both 1.5 and 3.0 T across both vendors, the ADC values ranged from $(1.12 \pm 0.01) \times 10^{-3} \text{ mm}^2/\text{s}$ for pure water to $(0.48 \pm 0.02) \times 10^{-3} \text{ mm}^2/\text{s}$ for the 25% w/w PVP concentration, exhibiting an anticipated decrease with the increase in PVP concentration. The differences in ADC values between the vendors and the field strengths were small.

3.B. IR- T_1 and T_2 relaxation times

The mean calculated IR- T_1 and T_2 relaxation times of each vial are presented in Tables VI and VII. In both cases, the relaxation times varied across the different acquisitions showing some variance with field strength and vendor, although generally a good agreement was found across the scanners for each gel concentration. T_2 relaxation times derived from 1.5 T data showed variation when compared to the corresponding values from 3.0 T data, whereas for the majority of the vials, the IR- T_1 relaxation times at 3.0 T demonstrate an increasing T_1 as compared to the 1.5 T

TABLE V. ADC ($\times 10^{-3} \text{ mm}^2/\text{s}$) estimates (median \pm s.d. of each ROI mean) of each PVP solution across the different scanners.

PVP concentration (% w/w)	ADC ($\times 10^{-3} \text{ mm}^2/\text{s}$)			
	A (1.5 T)	B (1.5 T)	C (3.0 T)	D (3.0 T)
0	1.12 ± 0.01	1.11 ± 0.02	1.12 ± 0.01	1.11 ± 0.01
2.5	1.05 ± 0.02	1.04 ± 0.02	1.08 ± 0.02	1.04 ± 0.01
5	0.98 ± 0.02	0.98 ± 0.01	1.01 ± 0.02	0.95 ± 0.01
10	0.85 ± 0.01	0.86 ± 0.01	0.86 ± 0.01	0.82 ± 0.01
15	0.71 ± 0.01	0.72 ± 0.02	0.71 ± 0.01	0.71 ± 0.01
20	0.59 ± 0.02	0.59 ± 0.01	0.59 ± 0.01	0.59 ± 0.01
25	0.50 ± 0.02	0.49 ± 0.01	0.49 ± 0.02	0.48 ± 0.02

TABLE VI. IR- T_1 (ms) relaxation times (median \pm s.d. of each ROI) of each PVP solution using the inversion recovery measurement across the different scanners.

PVP concentration (% w/w)	IR- T_1 (ms)			
	A (1.5 T)	B (1.5 T)	C (3.0 T)	D (3.0 T)
0	1415 \pm 19	1520 \pm 26	1562 \pm 17	1488 \pm 28
2.5	1398 \pm 24	1380 \pm 24	1449 \pm 11	1376 \pm 22
5	1313 \pm 13	1251 \pm 21	1328 \pm 14	1252 \pm 21
10	1098 \pm 15	1041 \pm 26	1105 \pm 13	1073 \pm 15
15	879 \pm 16	872 \pm 15	913 \pm 13	905 \pm 13
20	664 \pm 14	688 \pm 14	761 \pm 15	745 \pm 11
25	523 \pm 15	543 \pm 16	609 \pm 18	612 \pm 13

values. The SNR of the T_2 -weighted images was estimated by drawing an ROI on the vial with the shortest T_2 within the longest-TE image and was found to be satisfactory at 492–1960 (signal/noise).

3.C. VFA- T_1 and dynamic measurement stability

The T_1 values derived from the VFA method, VFA- T_1 , are presented in Table VIII and show a large variation from those derived by the (gold-standard) inversion recovery method, with larger variance across scanners as well as for repeated measurements on each scanner. Scanner C gives consistently higher T_1 estimates for VFA than for IR- T_1 , with the other scanners in general agreement. The standard deviation seen in the VFA- T_1 estimate across each individual ROI, Table IX, are relatively small, indicating a stable dynamic series of images, with the main source of variation being in T_1 estimation across separate scanning sessions. In all cases, the average mean/(standard deviation) of each T_1 estimate within the ROIs was greater than 20 (Table X).

The next-value autocorrelation of the dynamic series, measuring stability of the signal over the dynamic time course, was observed to be close to 0 (range -0.06 to 0.02) for all PVP concentrations in three out of four scanners, with the final scanner (Scanner D, 3.0 T) returning values consistently higher and indicating instability in the signal over time (Table XI). Examination of one such

TABLE VII. T_2 (ms) relaxation times (median \pm s.d. of each ROI) of each PVP solution in the phantom measured across the different scanners.

PVP concentration (% w/w)	T_2 (ms)			
	A (1.5 T)	B (1.5 T)	C (3.0 T)	D (3.0 T)
0	1403 \pm 3	1417 \pm 5	1511 \pm 11	1433 \pm 11
2.5	1281 \pm 2	1334 \pm 6	1396 \pm 10	1323 \pm 8
5	1277 \pm 8	1201 \pm 4	1247 \pm 10	1171 \pm 4
10	1046 \pm 3	984 \pm 2	985 \pm 4	941 \pm 4
15	841 \pm 3	811 \pm 3	791 \pm 5	760 \pm 6
20	638 \pm 4	661 \pm 3	638 \pm 7	608 \pm 6
25	512 \pm 4	526 \pm 4	509 \pm 5	490 \pm 7

TABLE VIII. Mean VFA- T_1 (ms) relaxation times (median \pm s.d. of each ROI) of each PVP solution calculated across the dynamic series.

PVP concentration (% w/w)	Mean VFA- T_1 (ms)			
	A (1.5 T)	B (1.5 T)	C (3.0 T)	D (3.0 T)
0	1520.4 \pm 311	1732.6 \pm 29	2344.7 \pm 330	1466.4 \pm 166
2.5	1217.1 \pm 224	1394.5 \pm 59	1759.5 \pm 165	1108.2 \pm 145
5	990.6 \pm 166	1214.5 \pm 46	1538.8 \pm 173	1050.6 \pm 141
10	762.7 \pm 139	866.1 \pm 9	1163.7 \pm 122	886.5 \pm 91
15	611.1 \pm 74	638.9 \pm 2	961.5 \pm 86	710.4 \pm 85
20	478.9 \pm 15	500.4 \pm 7	724.2 \pm 72	569.4 \pm 87
25	399.7 \pm 32	412.4 \pm 12	576.0 \pm 32	459.6 \pm 85

example reveals a periodic variation in signal of around 15% (Fig. 3), and the correlogram shows a clear periodicity of around 38 s.

3.D. Repeatability measurements

The short-term and long-term repeatability estimates, assessed by calculating of the coefficient of variation for each case, are given for each parameter in Table XII. Excellent repeatability of 5% or lower, often below 1%, was observed across all scanners for both long-term and short-term comparisons of ADC, T_2 , and IR- T_1 values. The short-term repeatability was almost always better than the long-term for these parameters.

Parameters derived from the dynamic data show consistently higher CoV, with values as high as 17% and 10% for long-term and short-term repeatability, respectively. While short term CoVs are generally smaller than long-term, the difference is often minor and suggests no fundamental difference from repetitions of measurements on the different timescales. Moreover, for each vendor the dependence of the ADC estimates with the morning and afternoon session was estimated in order to investigate any effect related to the time of the scanning session. In all cases, the ADC CoVs between the morning and the afternoon measurement were less than 2%.

TABLE IX. Median standard deviations with the standard deviation of each calculation of VFA- T_1 relaxation times in each ROI across the dynamic series.

PVP concentration (% w/w)	Median standard deviations of VFA- T_1			
	A (1.5 T)	B (1.5 T)	C (3.0 T)	D (3.0 T)
0	64.1 \pm 23	65.6 \pm 2	50.5 \pm 22	30.8 \pm 6
2.5	38.6 \pm 19	43.0 \pm 2	34.6 \pm 20	19.9 \pm 4
5	26.4 \pm 14	24.2 \pm 1	26.0 \pm 17	17.0 \pm 3
10	17.8 \pm 9	17.9 \pm 2	18.3 \pm 12	12.7 \pm 1
15	15.4 \pm 3	12.6 \pm 1	16.8 \pm 11	10.5 \pm 2
20	10.3 \pm 1	7.1 \pm 1	12.6 \pm 8	8.7 \pm 2
25	8.6 \pm 0	6.1 \pm 1	10.3 \pm 7	7.3 \pm 2

TABLE X. Mean/standard deviation with the standard deviation of each calculation for T_1 relaxation times derived from VFA method.

PVP concentration (% w/w)	Mean/standard deviation			
	A (1.5 T)	B (1.5 T)	C (3.0 T)	D (3.0 T)
0	24.7 ± 3.3	26.1 ± 0.7	53.1 ± 23.5	48.9 ± 9.4
2.5	37.3 ± 12.3	32.4 ± 1.5	62.6 ± 30.4	58.5 ± 15.4
5	41.7 ± 12.3	50.1 ± 0.4	76.2 ± 41.0	64.0 ± 12.2
10	46.8 ± 11.7	48.9 ± 5.9	81.8 ± 42.0	70.3 ± 9.1
15	39.8 ± 2.8	51.5 ± 3.6	73.7 ± 38.1	68.0 ± 13.6
20	47.0 ± 5.2	72.3 ± 9.2	73.9 ± 39.7	67.5 ± 18.9
25	44.1 ± 2.6	70.8 ± 8.1	72.6 ± 38.2	67.1 ± 18.5

TABLE XI. Autocorrelation with the standard deviation of each calculation of dynamic data signal intensity with succeeding point.

PVP concentration (% w/w)	Autocorrelation			
	A (1.5 T)	B (1.5 T)	C (3.0 T)	D (3.0 T)
0	-0.03 ± 0.024	-0.06 ± 0.001	0.02 ± 0.022	0.29 ± 0.199
2.5	-0.05 ± 0.008	-0.04 ± 0.026	-0.02 ± 0.025	0.26 ± 0.260
5	-0.01 ± 0.024	-0.05 ± 0.024	-0.02 ± 0.030	0.33 ± 0.150
10	-0.03 ± 0.039	-0.05 ± 0.025	-0.02 ± 0.024	0.25 ± 0.191
15	-0.01 ± 0.017	-0.05 ± 0.013	-0.02 ± 0.075	0.23 ± 0.138
20	0.01 ± 0.008	-0.02 ± 0.041	0.01 ± 0.028	0.33 ± 0.283
25	-0.01 ± 0.014	-0.10 ± 0.014	0.00 ± 0.015	0.31 ± 0.179

4. DISCUSSION

This study presents a new phantom containing multiple compartments of PVP solutions at ice-water temperatures for the quality assurance of functional and quantitative imaging across different MRI platforms. The preparation of PVP solutions at different concentrations provides a physiologically relevant range of ADC and T_1 values, and with a range of T_2 values that can be measured to assess reliability, repeatability, and reproducibility in a multicenter setting using a standardized acquisition. The design of the phantom combines the features of existing alternative phantoms, including a chemically stable gel with user-modifiable MR properties, multiple compartments allowing the coverage of a wide MR parameter range, and known and reproducible temperature, to create a new phantom with all the conferred advantages.

There are several limitations in this study; first, scanners from only two different vendors were used, and this could be usefully expanded in future studies. Second, measurements were performed at both field strengths only for one vendor, allowing investigation of the influence of field strength only for this particular vendor. Finally, the DCE-MRI protocols in this study are not directly comparable, each implementation being a typical protocol for that platform, and thus allowing only assessment of their repeatability and variability. While this is not ideal, the primary scope of this study is not

to compare scanner performance, but the presentation of a phantom for the quality assurance of functional and quantitative imaging protocols allowing assessment of their reproducibility across multicenter studies.

The ADC values of this phantom are consistent with a variety of biological tissues (brain, bone marrow, and tumor), delivering a relevant physiological range, although the ADC range available is limited by the temperature control at 0 °C, and some tissues have larger ADC values (e.g., kidney). The excellent repeatability of the ADC measurements for both long and short term, assessed via calculation of the CoVs, indicates a reliable quality assurance procedure. Previous published repeatability of ADC measurements in phantoms^{12,15,16,24,25} are in agreement with our values.

The calculated ADC values across the MR scanners depicted differences between the vendors, in line with another phantom study.²⁵ In contrast to the study by Lavdas *et al.*²⁵ the ADC values reported in this study did not show any dependence with the field strength; the use of 7 different solutions in this study, compared to only 3, increases the confidence of the comparison. Malyarenko *et al.*¹⁵ report repeatability and reproducibility of a single ADC value in an ice-water phantom across different vendors and field strengths. With 3.0 T MR scanners becoming increasingly common, the utilization of a standardized quality assurance procedure across scanners of different field strength and vendor is crucial

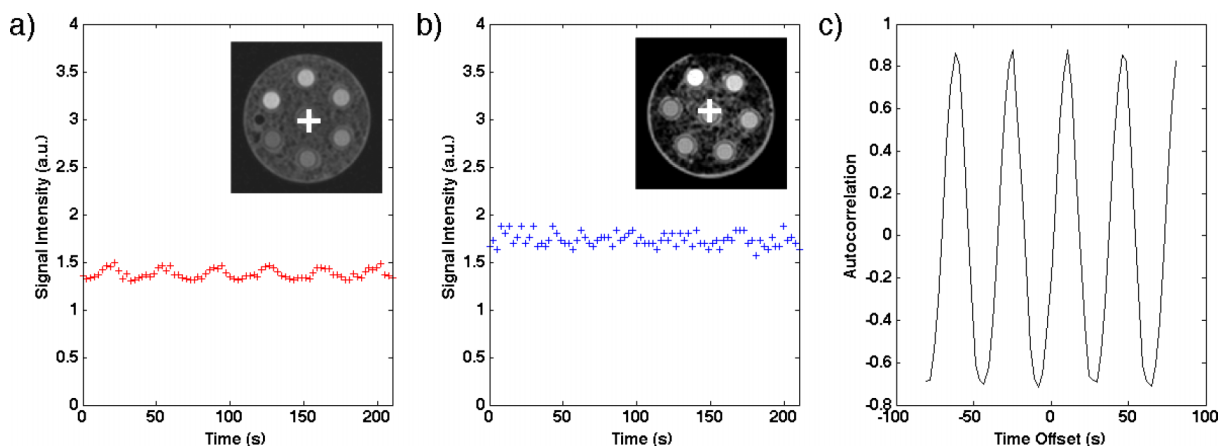


FIG. 3. Signal intensity trace within the 0% PVP vial (voxel locations shown inset), showing (a) unstable (scanner D) and (b) stable (scanner B) behavior; correlogram of scanner D data in (c) shows a periodicity of around 38 s.

TABLE XII. Coefficients of variations (%) for all derived parameters in each MRI scanner.

	A (1.5 T)		B (1.5 T)		C (3.0 T)		D (3.0 T)	
	Long-term	Short-term	Long-term	Short-term	Long-term	Short-term	Long-term	Short-term
ADC	0.9	1.1	1.3	0.7	1.1	0.4	1.1	1.0
T_2	5	0.6	0.6	0.2	0.3	0.3	0.3	0.5
IR- T_1	1.2	0.3	1.0	1.0	0.4	0.4	0.6	0.6
VFA- T_1 mean	7.51	0.74	2.23	1.63	3.49	2.47	3.52	4.47
VFA- T_1 mean/s.d.	16.91	6.10	8.65	6.36	7.29	5.77	11.76	8.71
AC	2.71	2.82	3.18	2.61	3.80	4.55	11.12	6.89
T_1 NF	6.69	0.47	1.68	1.07	3.56	2.21	1.46	2.28
T_1 SNR	15.74	2.28	9.89	7.70	7.40	5.40	10.66	9.32

for quality assurance in multicenter studies. In this study, not only repeatable DW measurements of multiple temperature-controlled solutions were presented but also quantitative T_1 , T_2 , and DCE-MRI measurements across two different vendors and field strengths.

The estimated values for IR- T_1 and T_2 relaxation times were comparable with the corresponding values of biological tissues and fluids, respectively.²⁶ It is both practical and convenient to acquire the T_1 and T_2 measurements under the same temperature control as required for reliable estimation of ADC, since these are also known to be sensitive to temperature.^{27,28} It is worth noting that T_1 values showed a dependence on the field strength, of approximately 40 ms/T for all vials (calculated as the average difference across field strengths for all the scanners), and this result is in agreement with the documented increase in T_1 values observed at 3.0 T by De Bazelaire.²⁶ Moreover, the good short-term and long-term repeatability (less than 5%) of these parameters using the protocol described demonstrates the reliability and repeatability of these measurements with this phantom.

Parameters derived from the dynamic scans, as used for DCE-MRI measurements, clearly demonstrate the difficulty with estimation of T_1 relaxation times using the variable flip angle measurements²⁹ and suggest that such data may only reliably provide relative T_1 values. The two-point VFA measurement works well for a single TR/ T_1 combination,³ but there is an inherent difficulty in accurate T_1 determination across a range of T_1 values; a multiple-flip angle measurement has been shown to improve T_1 accuracy but only at the expense of time.^{30,31} In the context of biomarkers for response, however, repeatability and stability of measurements are critical in being able to confidently identify changes in T_1 relaxation times, in clinical applications where the change may be small. The autocorrelation functions for the dynamic data showed acceptable stability across the varying PVP concentrations (with corresponding T_1 range) for all scanners over the acquisitions, with the exception of one scanner where the quality assurance procedure identified a periodic signal variation that would compromise the DCE-MRI study, which was not observed from a simple examination of T_1 standard deviation across the series. The CoV of dynamic parameters were consistently higher than those for ADC, IR- T_1 values, and T_2 , which reflects the compromise in data quality necessary when acquiring at high temporal resolution, though the CoVs

returned were shown to be acceptable (<10%) for both long-term and short-term repeatability.

In conclusion, the combination of a novel PVP phantom, with multiple compartments to give a physiologically relevant range of ADC and T_1 values, together with the simplicity and reproducibility of ice-water temperatures, allows reliable quality assurance measurements that can be used to measure agreement of MR scanners, which will be critical in the context of multicenter functional imaging studies that contain diffusion-weighted imaging, dynamic contrast-enhanced imaging, and T_1 and T_2 measurements.

ACKNOWLEDGMENTS

The research leading to these results has received support from the Innovative Medicines Initiative Joint Undertaking (www.imi.europa.eu) under Grant Agreement No. 115151, resources of which are composed of financial contribution from the European Union's Seventh Framework Programme (FP7/2007-2013) and EFPIA companies' in kind contribution. Certain commercial products are identified to specify the experimental study adequately. This does not imply endorsement by NIST or that the products are the best available for the purpose. N.P.J. is funded by Imagine for Margo. M.O.L. is a NIHR Senior Investigator. The authors acknowledge CR-UK and EPSRC support to the Cancer Imaging Centre at ICR and RMH in association with MRC and Department of Health Nos. C1060/A10334 and C1060/A16464, NHS funding to the NIHR Biomedicine Research Centre, the Clinical Research Facility in Imaging, and the CR-UK and EPSRC Paediatric Imaging Programme No. C7809/A10342.

CONFLICT OF INTEREST DISCLOSURE

The authors have no COI to report.

^{a)}N. P. Jerome and M.-V. Papoutsaki contributed equally to this work.

^{b)}Author to whom correspondence should be addressed. Electronic mail: Vasia.Papoutsaki@icr.ac.uk; Telephone: 020-8661-3718; Fax: 020-8661-0846.

¹D. M. Patterson, A. R. Padhani, and D. J. Collins, "Technology insight: Water diffusion MRI—a potential new biomarker of response to cancer therapy," *Nat. Clin. Pract. Oncol.* **5**(4), 220–233 (2008).

- ²A. R. Padhani *et al.*, "Diffusion-weighted magnetic resonance imaging as a cancer biomarker: Consensus and recommendations," *Neoplasia* **11**(2), 102–125 (2009).
- ³H. Z. Wang, S. J. Riederer, and J. N. Lee, "Optimizing the precision in T₁ relaxation estimation using limited flip angles," *Magn. Reson. Med.* **5**(5), 399–416 (1987).
- ⁴J. M. Froehlich *et al.*, "Diffusion-weighted MR imaging of upper abdominal organs: Field strength and intervendor variability of apparent diffusion coefficients," *Radiology* **270**(2), 454–463 (2014).
- ⁵C. P. Corona-Villalobos *et al.*, "Agreement and reproducibility of apparent diffusion coefficient measurements of dual-b-value and multi-b-value diffusion-weighted magnetic resonance imaging at 1.5 Tesla in phantom and in soft tissues of the abdomen," *J. Comput. Assist. Tomogr.* **37**(1), 46–51 (2013).
- ⁶H. Schmidt and P. Martirosian, "Impact of measurement parameters on apparent diffusion coefficient quantification in diffusion-weighted-magnetic resonance imaging," *Invest. Radiol.* **50**(1), 46–56 (2015).
- ⁷D. M. Chase *et al.*, "Changes in tumor blood flow as measured by dynamic contrast-enhanced magnetic resonance imaging (DCE-MRI) may predict activity of single agent bevacizumab in recurrent epithelial ovarian (EOC) and primary peritoneal cancer (PPC) patients: An exploratory," *Gynecol. Oncol.* **126**(3), 375–380 (2012).
- ⁸S. De Bruyne *et al.*, "Value of DCE-MRI and FDG-PET/CT in the prediction of response to preoperative chemotherapy with bevacizumab for colorectal liver metastases," *Br. J. Cancer* **106**(12), 1926–1933 (2012).
- ⁹K. Miyazaki *et al.*, "Neuroendocrine tumor liver metastases: Use of dynamic contrast-enhanced MR imaging to monitor and predict radiolabeled octreotide therapy response," *Radiology* **263**(1), 139–148 (2012).
- ¹⁰C. Messiou *et al.*, "Advanced solid tumors treated with cediranib: Comparison of dynamic contrast-enhanced MR imaging and CT as markers of vascular activity," *Radiology* **265**(2), 426–436 (2012).
- ¹¹P. S. Tofts *et al.*, "Test liquids for quantitative MRI measurements of self-diffusion coefficient *in vivo*," *Magn. Reson. Med.* **43**(3), 368–374 (2000).
- ¹²C. Pierpaoli, J. Sarlls, and U. Nevo, "Polyvinylpyrrolidone (PVP) water solutions as isotropic phantoms for diffusion MRI studies," in *Proceedings of the 17th of International Society for Magnetic Resonance in Medicine*, 2009, presentation number 1414.
- ¹³I. Delakis, E. M. Moore, M. O. Leach, and W. J. P. De, "Developing a quality control protocol for diffusion imaging on a clinical MRI system," *Phys. Med. Biol.* **49**, 1409–1422 (2004).
- ¹⁴M. Hara *et al.*, "A new phantom and empirical formula for apparent diffusion coefficient measurement by a 3 Tesla magnetic resonance imaging scanner," *Oncol. Lett.* **8**, 819–824 (2014).
- ¹⁵D. I. Malyarenko *et al.*, "Multi-system repeatability and reproducibility of apparent diffusion coefficient measurement using an ice-water phantom," *J. Magn. Reson. Imaging* **37**(5), 1238–1246 (2013).
- ¹⁶M. A. Boss *et al.*, "Temperature-controlled isotropic diffusion phantom with wide range of apparent diffusion coefficients for multicenter assessment of scanner repeatability and reproducibility," in *Proceedings of the 22nd of International Society for Magnetic Resonance in Medicine*, 2014, presentation number 4505.
- ¹⁷M. Freed *et al.*, "An anthropomorphic phantom for quantitative evaluation of breast MRI," *Med. Phys.* **38**(2), 743–753 (2011).
- ¹⁸E. K. Fram *et al.*, "Rapid calculation of T₁ using variable flip angle gradient refocused imaging," *Magn. Reson. Imaging* **5**(3), 201–208 (1987).
- ¹⁹K. Miyazaki, D. J. Collins, D.-M. Koh, D. J. Hawkes, M. O. Leach, and M. R. Orton, "Derivation of optimal flip angles via minimization of noise factor over large range of T₁ for accurate variable flip angles-derived T₁ estimation," *Proceedings of the 16th International Society for Magnetic Resonance in Medicine*, 2008, presentation number 1410.
- ²⁰J. Kurland, "Strategies and tactics in NMR imaging relaxation time measurements. I. Minimizing relaxation time errors due to image noise—the ideal case," *Magn. Reson. Med.* **15**, 136–158 (1985).
- ²¹J. Imran, F. Langevin, and H. Saint-Jalmes, "Two-point method for T₁ estimation with optimized gradient-echo sequence," *Magn. Reson. Imaging* **17**(9), 1347–1356 (1999).
- ²²O. N. Keene, "The log transform is special," *Stat. Med.* **14**(8), 811–819 (1995).
- ²³J. M. Bland and D. G. Altman, "Statistical methods in medical research," *Stat. Methods Med. Res.* **8**, 135–160 (1999).
- ²⁴M. E. Miquel, D. Scott, N. D. Macdougall, R. Boubertakh, N. Bharwani, and A. G. Rockall, "*In vitro* and *in vivo* repeatability of abdominal diffusion weighted MRI," *Br. J. Radiol.* **85**, 1507–1512 (2012).
- ²⁵I. Lavdas, M. E. Miquel, D. W. McRobbie, and E. O. Aboagye, "Comparison between diffusion-weighted MRI (DW-MRI) at 1.5 and 3 Tesla: A phantom study," *J. Magn. Reson. Imaging* **40**(3), 682–690 (2014).
- ²⁶C. M. J. De Bazelaire, G. D. Duhamel, N. M. Rofsky, and D. C. Alsop, "MR imaging relaxation times of abdominal and pelvic tissues measured *in vivo* at 3.0 T: Preliminary results," *Radiology* **230**(3), 652–659 (2004).
- ²⁷J. Simpson and H. Carr, "Diffusion and nuclear spin relaxation in water," *Phys. Rev.* **111**(5), 1201–1202 (1958).
- ²⁸P. M. Walker, C. Balmer, S. Ablett, and R. A. Lerski, "A test material for tissue characterisation and system calibration in MRI," *Phys. Med. Biol.* **34**(1), 5–22 (1989).
- ²⁹K. Miyazaki, J. D'Arcy, M. R. Orton, D.-M. Koh, D. J. Collins, and M. O. Leach, "Improved T₁ quantification using post-Gd contrast variable flip angle data," in *Proceedings of the 17th of International Society for Magnetic Resonance in Medicine*, 2011, presentation number 1092.
- ³⁰H.-L.M. Cheng and G. A. Wright, "Rapid high-resolution T₁ mapping by variable flip angles: Accurate and precise measurements in the presence of radiofrequency field inhomogeneity," *Magn. Reson. Med.* **55**, 566–576 (2006).
- ³¹S. C. L. Deoni, B. K. Rutt, and T. M. Peters, "Rapid combined T₁ and T₂ mapping using gradient recalled acquisition in the steady state," *Magn. Reson. Med.* **49**, 515–526 (2003).